ChemComm

# Electrocatalytic and photocatalytic hydrogen evolution integrated with organic oxidation

| Journal: | *ChemComm* |
|---|---|
| Manuscript ID | CC-FEA-03-2018-001830.R1 |
| Article Type: | Feature Article |
|  |  |

SCHOLARONE™
Manuscripts

# Journal Name

## ARTICLE

## Electrocatalytic and photocatalytic hydrogen evolution integrated with organic oxidation

Bo You[†], Guanqun Han[†], and Yujie Sun∗

Renewable energy-driven hydrogen production from electrocatalytic and photocatalytic water splitting has been widely recognized as a promising approach to utilize green energy resources and hence reduces our dependence on legacy fossil fuels as well as alleviates net carbon dioxide emission. The realization of large-scale water splitting, however, is mainly impeded by its slow kinetics, particularly because of its sluggish anodic half reaction, the oxygen evolution reaction (OER), whose product $O_2$ is ironically not of high value. In fact, the co-production of $H_2$ and $O_2$ in conventional water electrolysis may result in the formation of explosive $H_2/O_2$ gas mixtures due to gas crossover and reactive oxygen species (ROS), both pose safety concerns and shorten the lifetime of water splitting cells. Within these considerations in mind, replacing OER with thermodynamically more favorable organic oxidation reactions is much preferred, which will not only substantially reduce the voltage input for $H_2$ evolution from water, avoid the generation of $H_2/O_2$ gas mixtures and ROS, but also possibly lead to co-production of value-added organic products on the anode. Indeed, such an innovative strategy for $H_2$ production integrated with valuable organic oxidation has attracted increasing attention in both electrocatalysis and photocatalysis. This feature article showcases the most recent examples along this endeavor. As examplified in the main text, the oxidative transformation of a variety of organic substrates, including alcohol, ammonia, urea, hydrazine, and biomass-derived intermediate chemicals, can be integrated with energy-efficient $H_2$ evolution. We specifically highlight the importance of oxidative biomass valorizations coupled with $H_2$ production, as biomass is the only green carbon source whose scale is comparable to fossil fuels. Finally, the remaining challenges and future opportunities are also discussed.

## 1. Introduction

The continuous economy development and increasing global population necessitate the steady growth of energy production. As the current energy sector is highly dependent on fossil fuels, including coal, oil, and natural gas, their limited reserves pose a risk for our long-term development.[1-3] In addition, the adverse effect of fossil fuel utilization has been well manifested by its detrimental impact on environment, climate, and health of our planet. Consequently, intense research efforts have been focused on the capture, conversion, storage, and utilization of sustainable and clean energy resources, like solar and wind.[4,5] It has been estimated that the energy of solar irradiation on the Earth's surface with 80 min is sufficient to meet the global energy demands for an entire year based on current consumption rate.[2] To address the intermittency issue of renewable energies like solar irradiation, electrocatalytic and photocatalytic $H_2$ generation from water have been considered as attractive approaches for renewable energy storage in the form of chemical bonds.[6-8] In this case, the produced $H_2$ can be stored and later used on demand via hydrogen fuel cells. Additionally, $H_2$ is also a commodity

Department of Chemistry and Biochemistry, Utah State University, Logan, Utah 84322, United States. E-mail: yujie.sun@usu.edu. Fax: +1-435-797-3390; Tel: +1-435-797-7608.
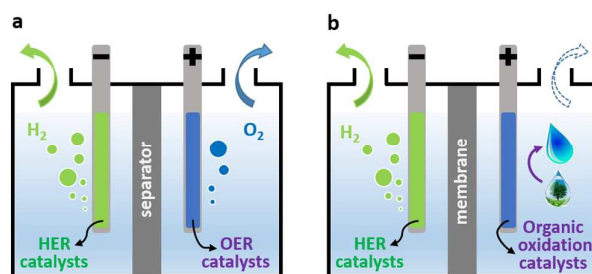
chemical in chemical industry.



**Fig. 1** Design of (a) conventional water splitting electrolyzer and (b) novel electrolyzer integrating $H_2$ evolution with organic oxidation.

As shown in Fig. 1a, conventional water electrolysis is usually conducted in strongly acidic electrolytes with noble metal-based catalysts (e.g., Pt for HER, and $IrO_2$ or $RuO_2$ for OER) and a proton exchange membrane (PEM) or in alkaline media using transition metal-based catalysts (e.g., Ni for HER and stainless steel for OER) and diaphragm.[9,10] In both cases, the $H_2$ and $O_2$ evolution reactions (HER and OER) are strictly coupled, which may lead to the formation of explosive $H_2/O_2$ mixtures due to gas crossover.[11-13] Gas crossover not only poses safety concern but also reduces the energy conversion efficiency as the crossed $O_2$ will be reduced back to water (acidic media) or hydroxide anion (alkaline media) on the cathode side.[9] In addition, the coexistence of $H_2/O_2$ gas

mixture and electrocatalysts may result in the formation of reactive oxygen species (ROS) which can degrade the membrane and thus shorten the lifetime of electrolyzer.[11] Another well-known limitation is that the four-electron/four-proton nature of OER requires much higher overpotential input than that of HER to afford the same current density, while the product $O_2$ is not very valuable. In fact, the voltage input for practical water splitting electrolyzers is always substantially larger than the thermodynamic potential of 1.23 V.

An alternative strategy for $H_2$ production from water is to replace the challenging but less valuable OER with thermodynamically favourable and economically more attractive organic oxidation reactions. Such a novel strategy will not only lower the voltage input, exclude the formation of $H_2/O_2$ gas mixture and ROS, but also produce more valuable organic products on the anode, maximizing the return of energy investment (Fig. 1b).

This Feature Article aims to present an overview of recent progress in electrocatalytic and photocatalytic $H_2$ generation integrated with various organic oxidations. A diverse array of organic substrates could be employed in this new strategy, ranging from alcohols,[14-18] ammonia,[19-21] urea,[22-25] hydrazine[26-28] to biomass-derived intermediate compounds[29-34] and others.[35-37]
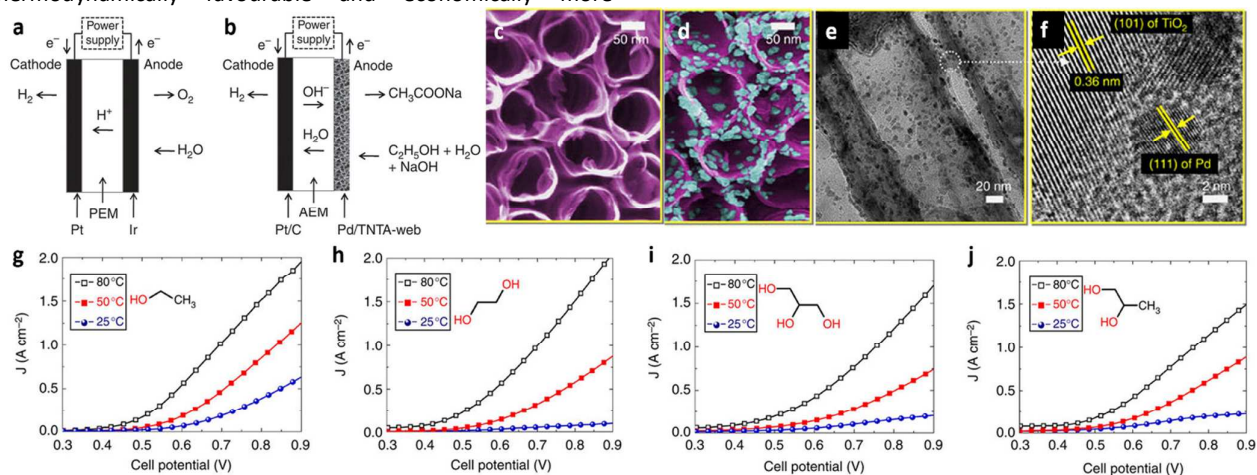


Fig. 2 Schematic of (a) PEM water electrolysis and (b) proposed alkaline water electrolysis. SEM images of (c) the bare 3D TNTA electrode support and (d) Pd/TNTA-web. (e) TEM and (f) HR-TEM images of Pd/TNTA-web. (g-j) Polarization curves for Pd/TNTA-web-based water electrolysis in 2 M NaOH solutions of (g) 2 M ethanol, (h) 2 M ethylene glycol, (i) 2 M glycerol, and (j) 2 M 1,2-propandiol under different temperatures. Reproduced from Ref. 14 with permission from Springer Nature, copyright 2014.

## 2. Electrocatalytic HER integrated with organic oxidation

Even though the thermodynamic potential of water splitting is only 1.23 V under standard condition, a cell voltage of 1.6 – 2.0 V is typically required to achieve current density larger than 1 mA cm$^{-2}$ in practical electrolyzers. Consequently, appreciable production of $H_2$ can only be obtained with an electrical energy consumption exceeding 45 kWh kg$^{-1}$ $H_2$. Because of the much lower standard thermodynamic potentials of alcohol oxidations than that of OER, Vitzza et al. demonstrated that it was feasible to replace OER with alcohol oxidation to produce $H_2$ with voltage less than 1 V, using palladium nanoparticles deposited on three-dimensional titania nanotube arrays (Pd/TNTA-web) as the anode electrocatalysts (Fig. 2a,b).[14] For the preparation of Pd/TNTA-web, commercial titanium non-woven sintered web support was anodized and annealed to form finely distributed titania nanotube arrays (TNTA), as confirmed by the scanning electron microscopy (SEM) image (Fig. 2c). Subsequently, a dipping-chemical reduction procedure was employed to deposit Pd nanoparticles. The SEM image in Fig. 2d clearly confirmed the homogeneous Pd distribution on the inner surface of TNTA. The TNTAs possessed an inner diameter of 100 nm with a wall thickness of 10 nm, and the Pd nanoparticles had an average particle size of ca. 13 nm (Fig. 2e). High-resolution transmission electron microscopy (HR-TEM) characterization also revealed the crystalline lattices of both anatase and the metallic Pd (Fig. 2f), further confirming the successful formation of Pd/TNTA-web. A two-electrode alkaline water electrolyzer was assembled using Pd/TNTA-web as the anode and Pt/C on carbon cloth as the cathode in 2 M NaOH (Fig. 2b). Fig. 2g showed the typical polarization curves obtained at 25, 50, and 80 $^{o}$C with 2 M ethanol. It is apparent that the output current density at a cell potential of 0.9 V at 80 $^{o}$C (1.95 A cm$^{-2}$) is more than three times higher than that at 25 $^{o}$C (0.51 A cm$^{-2}$), mainly due to the enhanced kinetics of ethanol oxidation along temperature increase. Similar results were obtained for other alcohols including ethylene glycol (Fig. 2h), glycerol (Fig. 2i) and 1,2-propandiol (Fig. 2j). It was calculated that the use of ethanol for $H_2$ production (18.5 kWh kg$^{-1}$ $H_2$) results in an electrical energy saving of 26.5 kWh kg$^{-1}$ $H_2$. Moreover, these alcohols can be produced from the fermentation of biomass or steam reforming of cellulosic materials with reasonably low energy cost,[14] and the corresponding products of organic acids are valuable than $O_2$.[34b] However, the utilization of Pd and Pt-based electrocatalysts inevitably leads to a high cost of the electrolyzer.

With this consideration in mind, we reasoned that it is economically more appealing to explore first-row transition metal-based electrocatalysts. Our group recently reported a 3D hierarchically porous nickel electrocatalyst (hp-Ni) for such an ? integrated water electrolysis.[33] The hp-Ni electrocatalyst was prepared by a facile template-free cathodic electrodeposition of highly porous Ni microspheres on a nickel foam at −3.0 A cm$^{-2}$ for 500 s. SEM images in Fig. 3a indicated the 3D hierarchically macroporous nature of hp-Ni with pore size of several hundred micrometers and abundant smaller macropores on the interconnected walls. Such a hierarchically porous structure is believed to facilitate the accessibility of catalytically active sites and mass transport for improved electrocatalytic performance.[38] Fig. 3b plotted the linear sweep voltammetry (LSV) curves of the oxidation of ethanol and water on hp-Ni in 1.0 M KOH. Upon the addition of 10 mM ethanol, the catalytic onset potential shifted from 1.51 V to 1.35 V vs. RHE and substantial anodic current density was observed within 1. 4 V vs. RHE, indicative of ethanol oxidation being easier than OER. In order to demonstrate the versatility of hp-Ni, we further extended the organic substrate group to benzyl alcohol (BA). Similar cathodic shift of the LSV curve was observed once BA was added in the electrolyte (Fig. 3c). Long-term electrolysis was conducted at 1.423 V vs. RHE, where no water oxidation would occur. The concentration evolution of BA and its oxidation products was analysed by high-performance liquid chromatography (HPLC) and plotted in Fig. 3d, clearly indicating the increase of benzoic acid while decrease of BA over passed charge. As an initial endeavour to explore the electronic effect in alcohol oxidation catalyzed by hp-Ni, two derivatives of benzyl alcohol with electron-withdrawing (4-nitrobenzyl alcohol, NBA) and -donating (4-methylbenzyl alcohol, MBA) substituents at the *para* position were subjected to similar electrocatalytic oxidation on hp-Ni. Interestingly, both LSV curves of these two new substrates took off at a quite similar potential in comparison to that of the parent benzyl alcohol (Fig. 3e), suggesting that the catalytic onset potential of these alcohol oxidations is primarily determined by the potential to achieve the desirable oxidation state of hp-Ni, rather than the intrinsic thermodynamics of alcohol oxidation. Such an integrated electrolyzer required a voltage of 1.58 V to afford 50 mA cm$^{-2}$, nearly 220 mV smaller than that of pure water splitting and other nonprecious electrocatalysts-based water electrolysis at same current density.[1c] Post-electrolysis characterization of hp-Ni after stability tests (named as post-BA hp-Ni) demonstrated its partial oxidation on the catalyst surface. For example, the high-resolution Ni 2p$_{3/2}$ XPS spectrum for the post-BA hp-Ni showed a decreased peak at 852.6 eV which could be ascribed to metallic Ni and an increased peak at 856.0 eV attributed to oxidized Ni species (Fig. 3f). Therefore, the real catalytically active sites for alcohol oxidation are most likely high-valent nickel species.[39]

In addition to alcohols,[14-18] ammonia,[19-21] and urea[22-25] were also explored for the integration with HER.[22-25] For instance, Qiao's group recently reported that small-sized MnO$_2$ ultrathin nanocrystals could act as efficient electrocatalysts for urea oxidation with excellent performance. The catalytic current density achieved by their MnO$_2$ electrocatalysts was even greater than that of Pt/C. The same group also explored the oxidation of urea catalyzed by a two-dimensional Ni-based metal organic framework (MOF), which led to a potential reduction of 280 mV compared to that of Pt/C to achieve 10 mA cm$^{-2}$.[23]
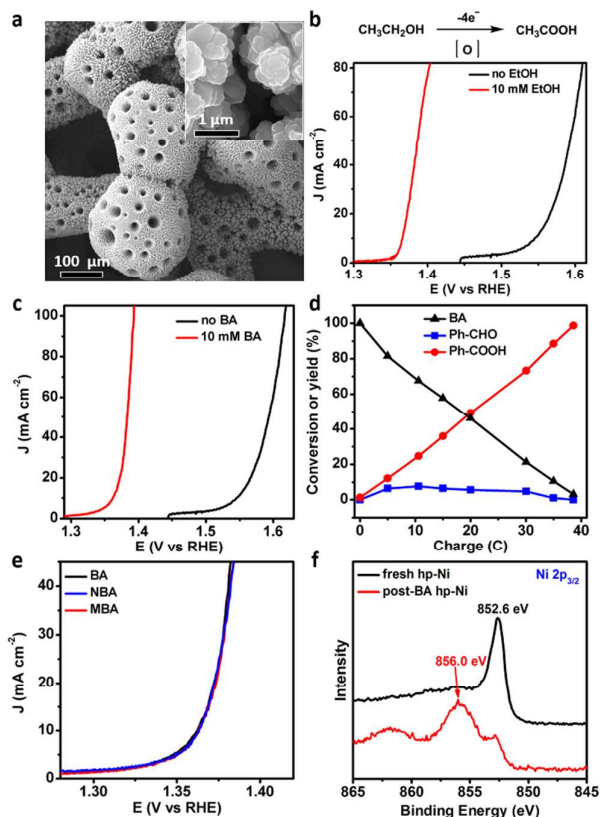


**Fig. 3** (a) SEM images of hp-Ni. (b) LSV curves for the oxidation of ethanol (EtOH, 10 mM) and water in 1.0 M KOH at 2 mV s$^{-1}$. (c) LSV curves of the oxidation of benzyl alcohol (BA, 10 mM) and water in 1.0 M KOH at 2 mV s$^{-1}$. (d) Benzyl alcohol conversion and product yield over passed charge during electrocatalysis at 1.423 V vs. RHE. (e) LSV curves of the oxidation of 10 mM benzyl alcohol (BA), 4-methylbenzyl alcohol (MBA), and 4-nitrobenzyl alcohol (NBA) on hp-Ni at 2 mV s$^{-1}$ in 1.0 M KOH. (f) High-resolution Ni 2p$_{3/2}$ XPS spectra of the fresh and post-BA hp-Ni electrocatalysts. Reproduced from Ref. 33 with permission from American Chemistry Society, copyright 2017.

The aforementioned electrocatalysis integrates H$_2$ production with different organic oxidations, resulting in potential saving of 200 − 300 mV relative to that of overall water splitting. However, a cell voltage of approximately 1.3 V is still needed to reach a meaningful current density like 10 mA cm$^{-2}$. It is highly desirable to explore other organic substrates to further reduce the voltage input for H$_2$ generation. Along this line, Sun and co-workers chose hydrazine oxidation as the counter reaction to couple HER using Ni$_2$P electrocatalyst coated on nickel foam (Ni$_2$P/NF).[26] The standard thermodynamic potential of hydrazine oxidation to N$_2$ is only -0.33 V.[26] As depicted in Fig. 4a, Ni$_2$P/NF featured interconnected nanosheet arrays with open network-like

nanostructure. The LSV curves of Ni$_2$P/NF with increasing hydrazine in 1.0 M KOH were compiled in Fig. 4b. In the absence of hydrazine, no oxidation current was observed within the potential window of -0.1 to 0.1 V vs. RHE. In contrast, the addition of 0.1 M hydrazine introduced a sharp current rise and increasing the hydrazine concentration from 0.1 to 0.5 M resulted in a rapid increase in oxidation current density, indicative of hydrazine oxidation catalyzed by Ni$_2$P/NF. As Ni$_2$P has been reported with high activity towards HER, Ni$_2$P/NF could function as a bifunctional electrocatalyst for H$_2$ production coupled with hydrazine oxidation. Consequently, an electrolyzer using Ni$_2$P/NF as both anode and cathode was then constructed. The Ni$_2$P/NF couple showed superior performance with a cell voltage of 1.0 V to afford 500 mA cm$^{-2}$ in 1.0 M KOH containing 0.5 M hydrazine (Fig. 4c). In the absence of hydrazine, a cell voltage of 1.6 V was required to reach 20 mA cm$^{-2}$ (Fig. 4d). A 10-h chronopotentiometry experiment revealed a relatively constant cell voltage requirement (0.45 V) to deliver 100 mA cm$^{-2}$ on Ni$_2$P/NF (Fig. 4e) together with nearly unity Faradaic efficiency (Fig. 4f). Collectively, these results demonstrated that replacing OER with hydrazine oxidation represents an effective way for efficient H$_2$ production with low voltage input.
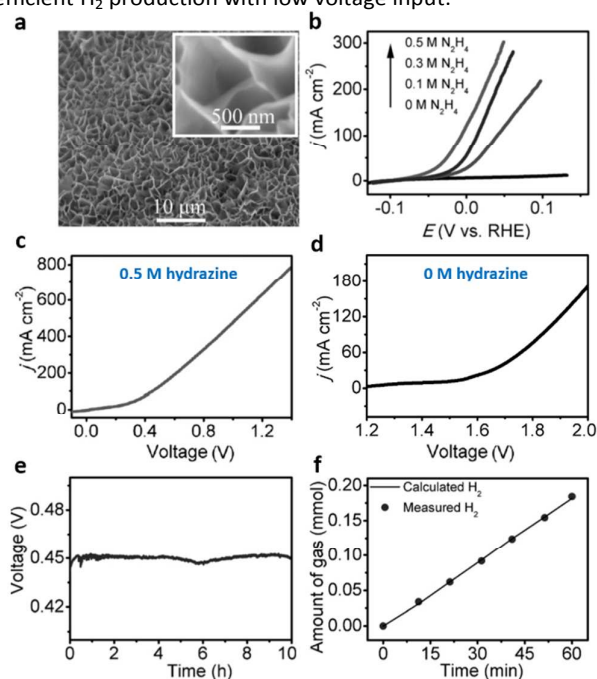


**Fig. 4** (a) SEM images of Ni$_2$P/NF. (b) LSV curves of hydrazine oxidation on Ni$_2$P/NF in 1.0 M KOH at 5 mV s$^{-1}$. LSV curves of Ni$_2$P/NF couple-based electrolysis in 1.0 M KOH at 5 mV s$^{-1}$ with a two-electrode configuration in the presence (c) and absence (d) of 0.5 M hydrazine. (e) Chronopotentiometric curve using a Ni$_2$P/NF catalyst couple to achieve a current density of 100 mA cm$^{-2}$ in 1.0 M KOH. (f) Gas chromatography-quantified and theoretical calculated H$_2$ amounts over electrolysis time. Reproduced from Ref. 26 with permission from John Wiley and Sons, copyright 2017.

Although the required voltage for such integrated electrolysis is dramatically reduced relative to that of conventional water electrolysis, the added organic substrates are consumed and transformed to low-value or even harmful by-products. For instance, urea oxidation produces N$_2$ and CO$_2$[22] and the oxidation of hydrazine consumes a high-energy fuel hydrazine to N$_2$.[40] Another problem that should not be overlooked is that these gaseous products may mix with the H$_2$ gas. Therefore, it is even more appealing to explore other organic oxidation reactions which can not only replace OER but also generate value-added and nongaseous products at the anode.

It is well-known that oxidative biomass upgrading holds a crucial role in converting biomass-derived feedstocks to many value-added chemicals.[29-34,41] Those oxygenated compounds can serve as primary building blocks to produce diverse commodities, polymers, and pharmaceuticals. Among many biomass-derived intermediates, 5-hydroxymethyl furfural (HMF) has been considered as one of the top biomass-derived platform chemicals. For example, one of its oxidation products, 2,5-furandicarboxylic acid (FDCA, Fig. 5a), is an important monomer to produce polyamides, polyesters, and polyurethanes, being a replacement of terephthalic acid.[29,42] Traditional approaches of biomass oxidation often involve stoichiometric chemical oxidants, elevated temperature, high temperature, and/or expensive catalysts. However, due to the increasing environmental regulations and economic concerns, efforts have been devoted to developing "green" catalytic processes, wherein catalysts only consist of earth-abundant elements while still possess high activity and robust stability under ambient conditions. In this regard, electrocatalytic oxidation offers an attractive strategy as it is only driven by electricity under ambient conditions and no chemical oxidants are necessary.

We recently reported a 3D Ni$_2$P nanoparticle arrays on Ni foam (Ni$_2$P NPA/NF) as a bifunctional electrocatalyst to couple H$_2$ production with HMF oxidation in alkaline media.[29] As revealed by the XRD and SEM measurements, 3D Ni$_2$P NPA/NF was successfully obtained (Fig. 5b,c). Similar to reported transition metal-based electrocatalysts for OER and alcohol oxidation,[33,43] an electrochemical activation phenomenon was also observed for Ni$_2$P NPA/NF during HMF oxidation, hence all the LSV curves in Fig. 5d were collected after the cessation of activation. In the presence of HMF, Ni$_2$P NPA/NF exhibited an onset potential of 1.35 V vs. RHE followed by a rapid current density rise within 1.40 V vs. RHE. While without HMF, the catalytic onset potential was shifted to 1.5 V vs. RHE and no appreciable current could be observed within 1.40 V vs. RHE, indicative of more favourable HMF oxidation than OER on Ni$_2$P NPA/NF (Fig. 5d). Chronoamperometry experiment was then carried out at 1.423 V vs. RHE and the concentration evolution of HMF and its oxidation products was monitored via HPLC measurements (Fig. 5e). Assuming a 100% Faradaic efficiency for the six-electron process of HMF oxidation to FDCA, 59 C was required to consume all the starting HMF. Indeed, as shown in Fig. 5e, after passing the theoretically calculated amount of charge, HMF nearly disappeared and the concentration of FDCA reached the maximum, confirming a nearly unity Faradaic efficiency for both HMF conversion and FDCA production. Even if an anion-exchange membrane was adopted, there still exist a possibility that HMF might migrate

to the cathode chamber and hence interfere HER on the cathode. Therefore, an ideal HER electrocatalyst should show great selectivity towards $H_2$ production in the presence of HMF. As an extreme case shown in Fig. 5f, the LSV curves of HER on $Ni_2P$ NPA/NF in the presence and absence of 10 mM HMF nearly overlapped, indicative of negligible influence of HMF on $H_2$ generation catalyzed by $Ni_2P$ NPA/NF.

After establishing the favourable HMF oxidation over OER and high selectivity of HER on $Ni_2P$ NPA/NF in the same electrolyte (1.0 M KOH with 10 mM HMF) under the three-electrode configuration, we next assembled a two-electrode electrolyzer for integrated HER and HMF oxidation using $Ni_2P$ NPA/NF as both anode and cathode. After introducing 10 mM HMF into the electrolyte (1.0 M KOH), the onset cell voltage was dramatically reduced (Fig. 5g). Fig. 5h presented that

nearly 200 mV voltage input was saved to reach benchmark current densities like 10, 20, and 50 mA cm$^{-2}$, highlighting the much better energy conversion efficiency of integrated HER and HMF oxidation relative to water splitting alone. Gas chromatography measurements further confirmed a nearly 100% Faradaic efficiency for $H_2$ production (Fig. 5i) and no $O_2$ was detected during the electrolysis at 1.50 V. Quantifying the resulting electrolyte by HPLC also resulted in a high Faradaic efficiency of ~97% for FDCA production. Such excellent Faradaic efficiencies for both HER and FDCA generation could be maintained for at least three consecutive electrolysis cycles employing the same $Ni_2P$ NPA/NF electrocatalyst couple (Fig. 5j). Collectively, these combined results undoubtedly proved the success of our proposed integrated electrolysis producing two valuable products ($H_2$ and FDCA) with lower energy input.
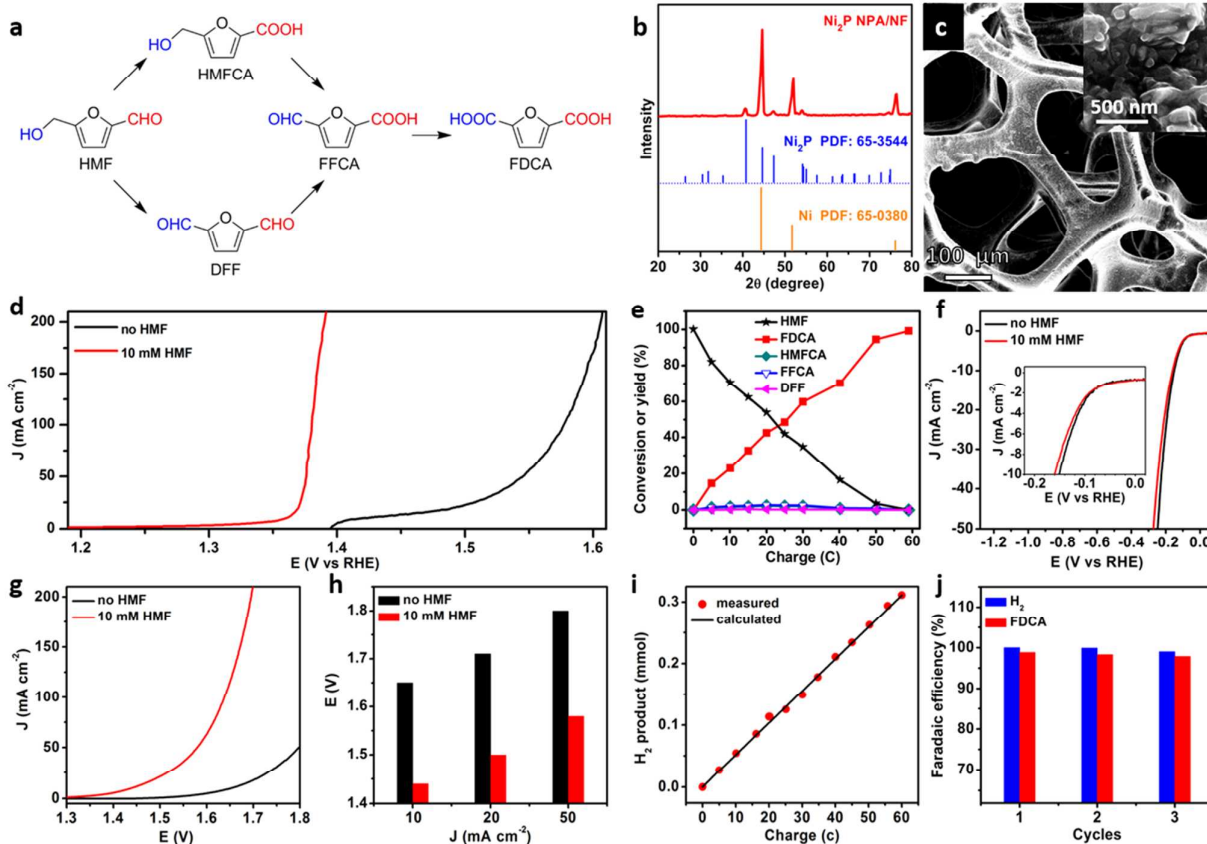


**Fig. 5** (a) Two possible pathways of HMF oxidation to FDCA. (b) XRD patterns and (c) SEM images of $Ni_2P$ NPA/NF. (d) LSV curves of $Ni_2P$ NPA/NF at 2 mV s$^{-1}$ in 1.0 M KOH with and without 10 mM HMF. (e) Conversion and yield changes of HMF and its oxidation products during the electrochemical oxidation of HMF at 1.423 V vs. RHE in 1.0 M KOH with 10 mM HMF. (f) LSV curves of $Ni_2P$ NPA/NF at 2 mV s$^{-1}$ in 1.0 M KOH with and without 10 mM HMF. (g) LSV curves and (h) comparison of the cell voltages to achieve benchmark current densities for a $Ni_2P$ NPA/NF catalyst couple in 1.0 M KOH with and without 10 mM HMF. (i) GC-measured $H_2$ quantity compared with that theoretically calculated amount assuming a 100% Faradaic efficiency. (j) Faradaic efficiencies of the $Ni_2P$ NPA/NF catalyst couple for simultaneous $H_2$ and FDCA generation in 1.0 M KOH solution with 10 mM HMF for three successive electrolysis cycles. Reproduced from Ref. 29 with permission from John Wiley and Sons, copyright 2016.

Encouraged by the above results, we further explored the electrocatalytic upgrading of various biomass-derived compounds like furfural and furfuryl alcohol on other nonprecious bifunctional electrocatalysts.[30] The high overpotential requirement of OER actually grants us a large potential window to perform various organic oxidation reactions catalyzed by low-cost electrocatalysts. For instance,

$Ni_3S_2$ could be adopted as a model electrocatalyst, which was prepared by straightforward sulfurization of commercially available nickel foams ($Ni_3S_2$/NF). Low-magnification SEM image of $Ni_3S_2$/NF indicated an interconnected macroporous 3D framework (Fig. 6a), similar to that of pristine Ni foam. Different from the featureless morphology of Ni foam, high-magnified SEM image of $Ni_3S_2$/NF revealed an interesting

structure composed of stacked nanoparticles (Fig. 6b,c). A close inspection of these nanoparticles in a high-resolution SEM image revealed the presence of abundant mesopores on the surface of $Ni_3S_2$/NF (Fig. 6b). Such a unique hierarchically porous nanostructure was expected to boost the accessibility of catalytically active sites and facilitate mass transport, beneficial to electrocatalytic performance.[38] Elemental mapping analysis of $Ni_3S_2$/NF confirmed the uniform distribution of Ni and S (Fig. 6d-f), validating the chemical conversion of Ni into $Ni_3S_2$. Five representative organic oxidation reactions were catalyzed by $Ni_3S_2$/NF in parallel. As complied in Fig. 6g-k, all the LSV curves in the presence of organic substrates universally took off at much lower potentials compared to those in the absence of organics, consistent with their more favourable oxidation relative to water oxidation. Interestingly, all the catalytic currents of organic oxidation rose at very similar potentials (~1.36 V vs. RHE), regardless of which organic substrate was oxidized. This phenomenon evokes a reminiscence of the oxidation of various benzyl alcohol derivatives catalyzed by hp-Ni (Fig. 3e). A two-electrode electrolyzer employing $Ni_3S_2$/NF as both

cathode and anode required a much lower voltage input for $H_2$ production coupled with HMF oxidation to achieve benchmark current densities (10, 20, 50, and 100 mA cm$^{-2}$) relative to pure water splitting electrolysis using the same electrode couple (Fig. 6l). For example, in order to produce a current density of 100 mA cm$^{-2}$, a voltage of 1.64 V was needed for the integrated electrolysis; while for overall water splitting electrolysis, 1.84 V was required to arrive at the same current density. Although the low-magnified SEM image (Fig. 6m) of post-HMF $Ni_3S_2$/NF indicated the maintenance of the overall 3D hierarchically porous configuration and primary $Ni_3S_2$ phase, high-magnification SEM images (Fig. 6n,o) revealed the presence of featureless monoliths, different from the pristine sample (Fig. 6 b,c). Elemental mapping images in Fig. 6p indicated that the post-HMF oxidation $Ni_3S_2$/NF mainly consisted of Ni and S, plus a large concentration of O over the newly formed monoliths, indicating the oxidation of $Ni_3S_2$ during electrolysis. In addition to these aforementioned examples, many other electrocatalytic systems have been explored for the coupled $H_2$ evolution and organic oxidation, which are summarized in Table 1.
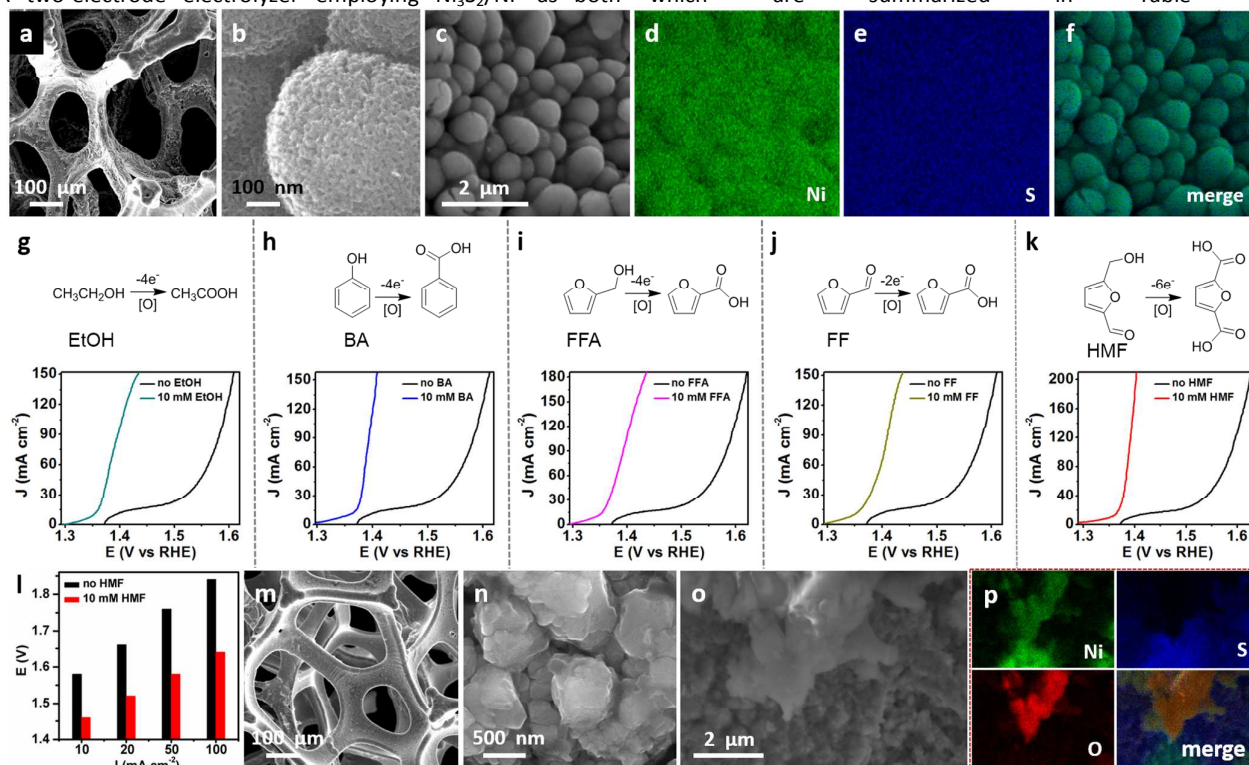


Fig. 6 (a-c) SEM images at different magnifications and (d-f) elemental mapping images of $Ni_3S_2$/NF. (g-k) LSV curves of selected organics (10 mM) to value-added products compared to water oxidation catalyzed by $Ni_3S_2$/NF at 2 mV s$^{-1}$ in 1.0 M KOH (EtOH: ethanol; BA: benzyl alcohol; FFA: furfuryl alcohol; FF: furfural; HMF: 5-hydroxymethylfurfural). (i) Comparison of the cell voltages to achieve benchmark current densities for a $Ni_3S_2$/NF catalyst couple in 1.0 M KOH with and without 10 mM HMF. (m-p) SEM images at different magnifications and elemental mapping images of $Ni_3S_2$/NF after HMF oxidation. Reproduced from Ref. 30 with permission from American Chemical Society, copyright 2016.

# Journal Name

## ARTICLE

**Table 1.** Representative electrocatalytic hydrogen evolution coupled with organic oxidation in aqueous media.

| Catalyst | Electrolyte | Organic substrate | Organic product | Three-electrode setup | | | Two-electrode setup | | FE (%) | | Ref. |
|---|---|---|---|---|---|---|---|---|---|---|---|
| | | | | $\eta_{HER}$ (V) | $\eta_{OER}$ (V) | $\eta_{organic}$ [a] | $V_1$ (V) [b] | $V_2$ (V) [c] | HER | Org. | |
| Pd/TNTA | 2.0 M NaOH | 2 M ethanol | acetic acid | - | - | - | 1.76 (1000) | 0.69 | - | - | [14] |
| F-β-FeOOH | 1.0 M KOH | ethanol:$H_2O$=15:5 | acetic acid | - | 1.59 | 1.207 | 1.51 | 1.43 | 91.7 | ~72 | [15] |
| Ni$_2$S/CFC | 1.0 M KOH | 0.45 M 2-propanol | acetone | -0.21 | 1.515 | 1.348 | - | - | 100 | 98 | [16] |
| NC@CuCo$_2$N$_x$/CF | 1.0 M KOH | 15 mM benzyl alcohol | benzaldehyde | -0.105 | 1.46 | 1.25 | 1.62 | 1.55 | 97.4 | ~81 | [17] |
| Co$_3$O$_4$ NSs/CP | 1.0 M KOH | 1 M ethanol | ethyl acetate | - | 1.50 | 1.445 | - | - | - | 98 | [18a] |
| 3D PdCu alloy | 1.0 M KOH | 1 M ethanol | ethyl acetate | -0.106 | - | 1.56 (onset) | - | - | - | - | [18b] |
| S-MnO$_2$/NF | 1.0 M KOH | 0.5 M urea | None | - | - | 1.33 | - | 1.41 | - | - | [22] |
| Ni$_2$P/NF | 1.0 M KOH | 0.5 M hydrazine | None | -0.29 (200) | - | 0.018 (200) | 1.6 (20) | 1.0 (500) | 100 | - | [26] |
| CoP/TiM | 1.0 M KOH | 0.1 M hydrazine | none | - | 1.55 (onset) | -0.05(onset) | 1.65 | 0.2 | 100 | - | [27] |
| Cu$_3$P/CF | 1.0 M KOH | 0.5 M hydrazine | none | -0.496 (100) | - | 0.152 (100) | 1.85 | 0.72 (100) | - | - | [28] |
| Ni$_2$P NPA/NF | 1.0 M KOH | 10 mM HMF | FDCA | -0.15 | 1.50 (onset) | 1.35 (onset) | 1.65 | 1.44 | 100 | 98 | [29] |
| Ni$_3$S$_2$/NF | 1.0 M KOH | 10 mM HMF | FDCA | -0.16 | 1.50 (onset) | 1.35 (onset) | 1.58 | 1.46 | 100 | 98 | [30] |
| Co-P/CF | 1.0 M KOH | 50 mM HMF | FDCA | - | 1.53 (20) | 1.38 (20) | 1.59 (20) | 1.44 (20) | 100 | - | [31] |
| Ni$_2$P/Ni/NF | 1.0 M KOH | 30 mM furfural | furoic acid | - | 1.55 (onset) | 1.43 (onset) | 1.59 | 1.48 | 100 | 100 | [32] |
| hp-Ni | 1.0 M KOH | 10 mM benzyl alcohol | benzoic acid | -0.219 (50) | 1.51 (onset) | 1.35 (onset) | 1.69 | 1.50 | 100 | 97 | [33] |
| Fe-CoP/CC | 1.0 M KOH | 5 mL aloe extract | - | -0.359 (100) | 1.707 (25) | 1.572 (25) | 1.57 | 1.44 | 100 | - | [34a] |
| CoP NWs/CC | 1.0 M KOH | 40 mg L$^{-1}$ triclosan | phenol | -0.069 | 1.59 | 1.54 | 1.68 | 1.63 | 100 | - | [35] |
| Fe$_2$P/SSM | 10 M KOH | 0.5 M glucose | - | - | 1.43 (onset) | 1.33 (onset) | 1.52 | 1.22 | 100 | - | [36] |
| Nano-Cu foam | 0.1 M KOH | 5 mM HMF | FDCA | - | 1.6 (onset) | 1.25 (onset) | - | - | 100 | 95.3 | [42b] |

[a] All the potentials are reported as V vs. RHE. If not indicated, the listed potentials are those to achieve 10 mA cm$^{-2}$. Numbers in parentheses are current densities in mA cm$^{-2}$. [b] $V_1$ is the cell voltage for pure water splitting. [c] $V_2$ is the cell voltage for the integrated HER with organic oxidation.

# Journal Name

## ARTICLE

### 3. Photocatalytic HER integrated with organic oxidation

Besides electrocatalytic $H_2$ production from water with electricity as the energy input, photocatalysis provides another more direct approach to convert and store solar energy in chemical bonds.[44] In fact, light-driven water splitting for $H_2$ evolution has attracted much research interest during the last few decades. Since the discovery of photoelectrochemical water splitting on $TiO_2$ in 1972,[47] extensive studies have been conducted for photo-driven $H_2$ evolution on semiconductors.[48] Generally, three steps are involved in semiconductor-based photocatalysis: (i) light absorption and photogeneration of electron-hole pairs, (ii) migration of photogenerated electron-hole pairs to respective sites, and (iii) charge utilization for $H_2$ production and another oxidation reaction. An ideal semiconductor should meet at least two criteria: suitable band gap for efficient light absorption and appropriate band positions for sufficient reducing and oxidizing power.

In order to minimize the recombination of excited electrons and holes upon light irradiation, sacrificial electron donors are usually employed in photocatalytic systems for $H_2$ production. However, such a conventional strategy not only increases the overall cost of $H_2$ production, but also wastes the oxidizing power of excited holes. Analogous to the scenario successfully demonstrated for integrated HER and organic oxidation in the aforementioned electrocatalytic systems, it is quite appealing to seek alternative organic oxidation reactions to consume the photogenerated holes on semiconductors while simultaneously produce value-added organic products. Recent years witness the emergence of such an integrated photocatalysis strategy for HER and organic reforming on several semiconductor systems, including carbon nitride and cadmium chalcogenides. Among various organic oxidation reactions, photo-driven oxidation of alcohols to aldehydes shows a great promise to be coupled with $H_2$ generation.[49,50,51]

#### 3.1 Carbon nitride-based photocatalysts

Carbon nitride ($CN_x$) has emerged as a great semiconductor during recent years because of its visible light absorption and well-positioned valence and conduction bands for many important redox reactions, including water splitting.[52] For instance, Sun et al. reported a hybrid photocatalyst system, utilizing $C_3N_4$ as the semiconductor, a ruthenium complex and platinum as the oxidation and reduction catalysts, respectively, for the photo-induced benzyl alcohol oxidation and $H_2$ evolution.[53] The presence of the molecular ruthenium catalyst remarkably improved the selectivity of benzyl alcohol

oxidation to benzylaldehyde primarily due to the formation of Ru(IV)=O active species. Similarly, Yang and his co-workers synthesized fibrous Ag nanoparticles decorated on g-$C_3N_4$ aerogel.[54] This photocatalytic system exhibited excellent photocatalytic performance for $H_2$ evolution in the presence of methanol, which was oxidized to formaldehyde. Nevertheless, the utilization of expensive metals (Pt, Ru, and Ag) in these photocatalytic systems inevitably results in high cost for large-scale applications. It is more desirable to explore non-precious alternatives.
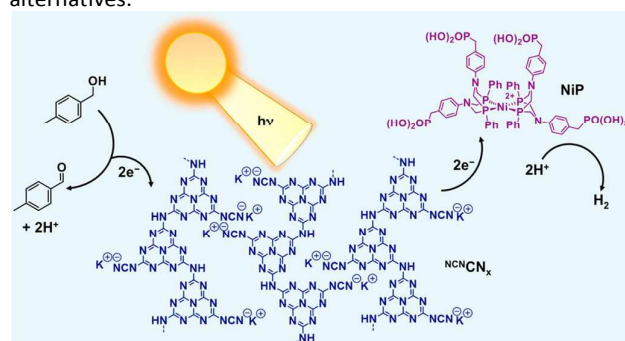


**Fig. 7** Schematic representation of a closed redox system for solar-driven $H_2$ evolution coupled with alcohol oxidation in aqueous media. Reproduced from Ref. 55 with permission from American Chemical Society, copyright 2016.

In 2016, Reisner et al. reported a hybrid photocatalytic system consisting of carbon nitride decorated with cyanamide on the surface and a molecular nickel(II) bis(diphosphine) catalyst to integrate light-driven $H_2$ evolution and benzylic alcohol oxidation (Fig. 7).[55] Under optimized conditions, such a hybrid system showed an high activity towards HER and aldehyde production with a rate of 763 µmol g$^{-1}$ h$^{-1}$ and a quantum efficiency of 15%. A turnover frequency of 76 h$^{-1}$ was calculated based on the amount of nickel and the conversion of 4-methylbenzyl alcohol arrived at 83.0%. Transient absorption spectroscopy studies demonstrated that the presence of cyanamide groups on the surface of carbon nitride was critical in that these groups would suppress the recombination of excited electrons and holes, leading to a higher production yield. Unfortunately, this hybrid system had a relatively short operational lifetime, most likely due to the poor stability of the nickel catalyst under photocatalysis conditions.

#### 3.2 Cadmium chalcogenides-based photocatalysts

Another popular semiconductor candidate for photocatalysis applications is CdS whose conduction band lies at -0.5 V vs. NHE and valence band at +1.9 V vs. NHE.[56,57,59] Feldmann's group reported an interesting CdS-based photocatalytic system utilizing a low-cost nickel co-catalyst for

$H_2$ production integrated with alcohol oxidation.[58] A unique redox shuttle mechanism was proposed. Under light irradiation, hydroxyl anions diffuse to the surface of CdS nanorods and are oxidized to hydroxyl radicals by excited holes. The in situ formed hydroxyl radicals later oxidize ethanol to acetaldehyde (Fig. 8a). The role of nickel nanoparticles was expected to catalyze $H_2$ evolution. The size and quantity of nickel nanoparticles on CdS could be conveniently controlled by photodeposition (Fig. 8b,c). The authors also investigated the pH influence on $H_2$ production. As shown in Fig. 8d, the amount of evolved $H_2$ was substantially larger at higher pH, probably due to fast alcohol oxidation along increasing alkalinity. The apparent quantum yield for $H_2$ production was measured as high as 49% over the first 20 h under irradiation with light wavelength of 447 nm. Longer photolysis resulted in lower quantum yield (~20%). Overall, such a hybrid photocatalytic system exhibited great stability, showing decent activity up to at least 220 h (Fig. 8e).
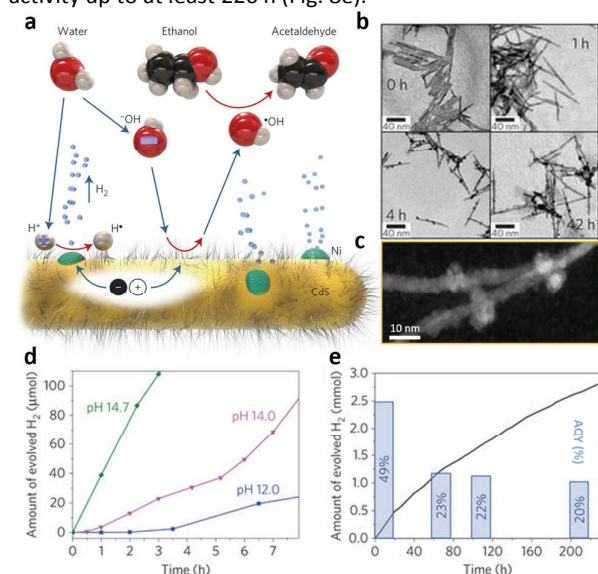


**Fig. 8** (a) Schematic of photocatalytic $H_2$ generation following a redox shuttle mechanism. (b) TEM images of CdS nanorods after photodeposition of nickel as a function of illumination time. (c) HAADF-STEM images of CdS decorated with nickel nanoparticles. (d) Amount of evolved $H_2$ vs. time at different pH. (e) Long-term $H_2$ evolution vs. illumination time with 10% ethanol. The bars denote the apparent quantum yield (AQY) at 447 nm averaged over 20 h of illumination. Reproduced from Ref. 58 with permission from Springer Nature, copyright 2014.

In order to increase the specific surface area and maximize the utilization of excited electrons and holes for photocatalysis applications, ultrathin two-dimensional (2D) nanosheet is a preferred morphology for semiconductors.[61,62] Last year, our group developed a microwave synthesis to prepare ultrathin 2D CdS nanosheets. With the assistance of the nickel co-catalyst, our Ni/CdS photocatalyst was able to drive $H_2$ evolution and organic upgrading under visible light irradiation.[63] After microwave treatment, the wurtzite crystal structure of CdS was obtained and no crystalline peaks due to nickel could be observed for Ni/CdS (Fig. 9a). The ultrathin thickness of Ni/CdS was measured at ~1.1 nm based on the atomic force microscopy (AFM) results in Fig. 9b. In contrast to previous studies where benzyl alcohol or ethanol was chosen as the organic substrates, our group was more interested in exploring photocatalytic upgrading of biomass-derived intermediate compounds coupled with $H_2$ evolution. In particular, we sought to conduct photo-induced valorization of furfural alcohol and HMF to furfural and 2,5-diformylfuran (DFF), respectively. As shown in Fig. 9c, under visible light irradiation, our 2D Ni/CdS nanosheets exhibited excellent performance for $H_2$ evolution when furfural alcohol was used as the organic substrate. In the meantime, furfural alcohol was converted to furfural with nearly 100% yield within 22 h irradiation (Fig. 9d). Surprisingly, when HMF was adopted as the organic substrate, much lower $H_2$ production rate was observed and it was not able to completely oxidize HMF to DFF after 22 h photolysis (yield ~22%), even though a similar oxidation from an alcohol group to an aldehyde group took place in both cases. The remarkable difference was further investigated via theoretical computations (Fig. 9e). It was rationalized that the binding affinity of the aldehyde group in HMF towards nickel oxide was slightly stronger than its alcohol group, therefore the aldehyde group more likely adsorbed on Ni/CdS while the alcohol group was kept away from the oxidizing sites, resulting in a slower oxidation of HMF to DFF. However, under alkaline conditions, both furfural alcohol and HMF were oxidized to their corresponding carboxylates with yields over 90%.

# Journal Name

## ARTICLE
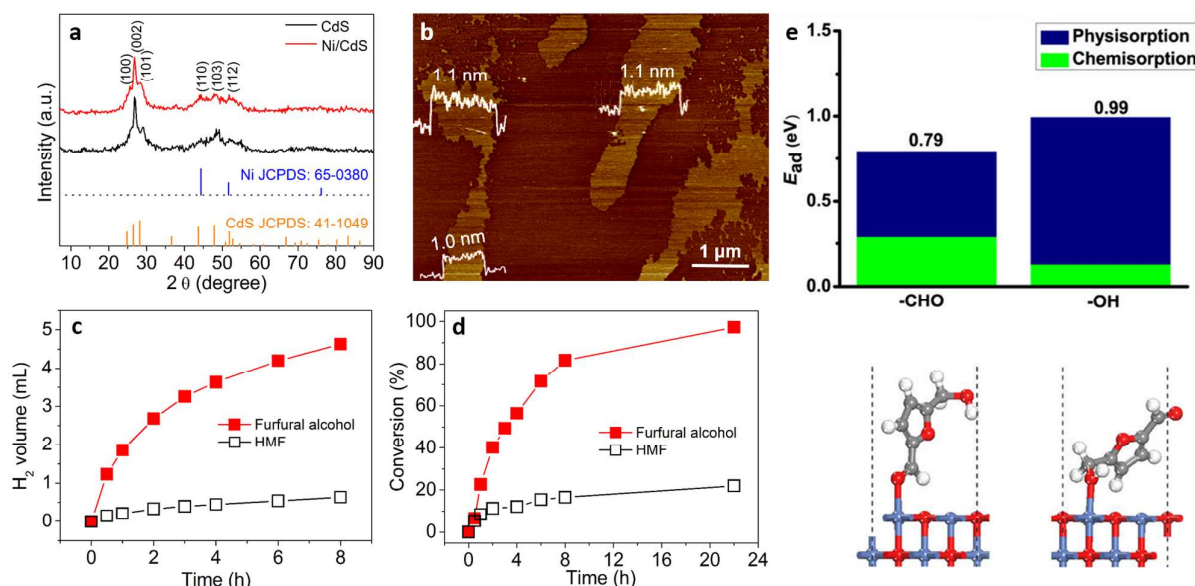


**Fig. 9** (a) XRD pattern and (b) AFM image of Ni/CdS. (c) Produced $H_2$ and (d) conversion of organic substrates during photocatalysis. (e) Adsorption structures and energies of HMF at water/NiO (001) interface via its aldehyde or alcohol group. Reproduced from Ref. 63 with permission from American Chemical Society, copyright 2017.

Given the great abundance of biomass as a sustainable and renewable carbon source, it remains a hot topic in exploring the direct conversion of biomass materials to value-added products, not only focusing on those biomass-derived small molecular intermediates but also cracking the stubborn polymeric components. As lignocellulose is one of the most prevalent biomass materials, increasing research efforts have been centered on its upgrading and utilization via green methods. Complex polymeric structures are involved in all the three main components of lignocellulose including cellulose, hemicellulose and lignin (Fig. 10a). Conventional biomass reforming processes usually require high temperature and expensive chemicals, which may result in carbon-based gaseous products like CO, $CO_2$, and $CH_4$. In contrast, visible light-driven reformation of lignocellulose to produce $H_2$ represents an alternative green approach. Last year, Reisner's group reported an interesting strategy for photo-induced $H_2$ production using lignocellulose and even raw biomass materials (Fig. 10b) as the hole scavengers to boost $H_2$ evolution, in which CdS quantum dots were utilized as the semiconductors.[60] Because of the quantum confinement effect, high specific surface area, and tunable band gap based on size, quantum dots possess enormous potential for photocatalysis.[64] In order to overcome the photo-corrosion of CdS quantum dots and simultaneously increase the solubility of biomass substrates, a highly alkaline electrolyte was applied, which was able to promote the formation of a

cadmium oxide ($CdO_x$) layer on the surface of CdS (Fig. 10c). It was found that the solution pH had a dramatic impact on $H_2$ evolution. As shown in Fig. 10d, increasing alkalinity resulted in higher $H_2$ production and the best activity was achieved in 10.0 M KOH when α-cellulose was used as the hole scavenger. Control experiment conducted in the absence of cellulose clearly proved the critical role played by cellulose in boosting $H_2$ yield, in that the addition of cellulose to the reaction solution dramatically enhanced the $H_2$ production rate by several magnitudes (Fig. 10e). In addition to α-cellulose, hemicellulose and lignin were also found to increase the $H_2$ production rate, albeit the performance of lignin was much lower than those of the former two substrates (Fig. 10f). The authors further tested several crude biomass materials, such as printer paper, cardboard, newspaper, wooden branch, grass, and sawdust (Fig. 10g), among which wooden branch demonstrated the best activity with a $H_2$ production rate over 5 mmol $g_{cat}^{-1}$ $h^{-1}$, which was even higher than those obtained from α-cellulose, ~2.3 mmol $g_{cat}^{-1}$ $h^{-1}$ (Fig. 10f). This seminal report highlighted the great promise of directly utilizing raw biomass materials to drive $H_2$ production with visible light irradiation under ambient conditions. Future efforts should focus on producing valuable chemicals from the oxidation of those raw biomass materials, rather than merely acting as hole scavengers for HER.

In addition to the aforementioned photocatalytic systems based on $CN_x$, and CdS, other robust semiconductors like CdSe,[65] Au-

ChemComm

**ARTICLE**

Pd/ZrO$_2$,[66] Ru/SrTiO$_3$:Rh,[67] and MgO[68] have also been applied in H$_2$ photogeneration coupled with organic oxidation reactions. For instance, Wu's group applied 3-mercaptopropionic-capped CdSe quantum dots to accomplish alcohol oxidation integrated with H$_2$ generation. A cascade catalytic cycle involving the generation of

thiol radical was proposed for their photocatalytic system. The in situ generated thiol radicals might be utilized for other complex organic reactions. A list of representative photocatalytic systems for the coupled H$_2$ evolution and organic oxidation is included Table 2.
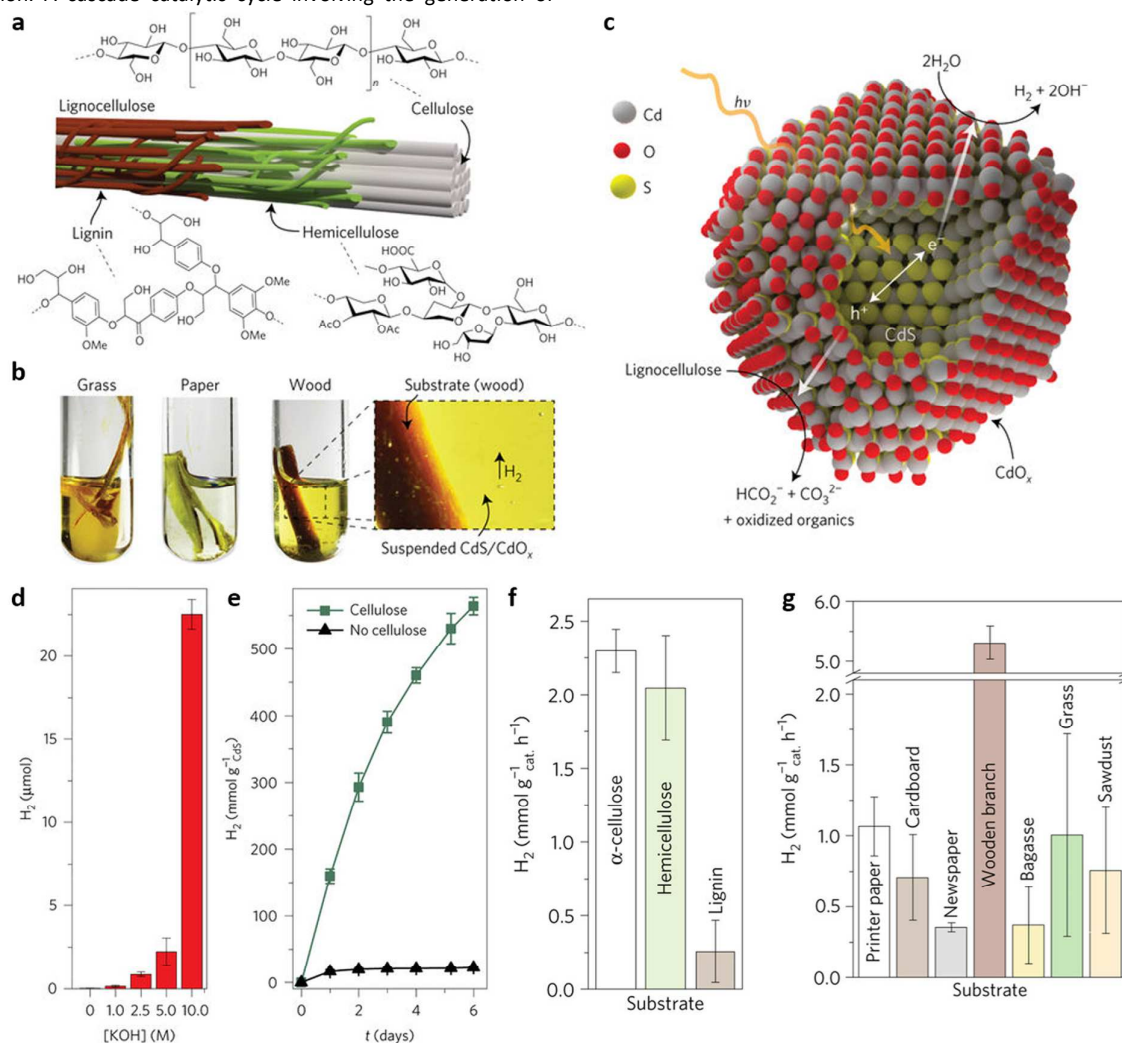


**Fig. 10** (a) Lignocellulose exists as microfibrils in plant cell walls and is comprised of cellulose surrounded by hemicellulose and lignin. (b) These components can be photo-reformed into H$_2$ using CdS coated with CdO$_x$. (c) This combination creates a highly robust photocatalyst capable of producing H$_2$ from lignocellulose when suspended in alkaline solution and irradiated with sunlight. (d) The pH dependence of the photocatalytic H$_2$ evolution from a 2 mL aqueous solution of ligand-free CdS (0.5 μM) with 50 mg mL$^{-1}$ α-cellulose after 18 h of irradiation. (e) Long-term photocatalytic cumulative production of H$_2$ by CdS (0.5 μM) with and without 50 mg mL$^{-1}$ α-cellulose in 2 mL KOH (10.0 M). Photocatalytic production of H$_2$ (AM 1.5G, 100 mWcm$^{-2}$) over 24 h with CdS (0.5 μM) and Co(BF$_4$)$_2$ (0.34 mM) in 2 mL KOH (10.0 M, 25 °C, anaerobic atmosphere) with (f) 50 mg α-cellulose mL$^{-1}$, 25 mg hemicellulose mL$^{-1}$ and 0.25 mg lignin mL$^{-1}$ and (g) 50 mg mL$^{-1}$ of raw and waste biomass substrates. Reproduced from Ref. 60 Springer Nature, copyright 2017.

# Journal Name

## ARTICLE

**Table 2.** Representative photocatalytic hydrogen evolution coupled with organic oxidation.

| Catalyst | Light source | Time (h) | Solvent | Substrate | Product | $H_2$ (µmol) | Conv. (%) | Sel. (%) | Ref. |
|---|---|---|---|---|---|---|---|---|---|
| $Pt/TiO_2$ | UV | 1 | $CH_3CN$ | benzyl alcohol | benzaldehyde | 48 | 99 | >99 | [50e] |
| $Pd/CdS-TiO_2$ | blue LED (460 nm, 10 mW cm$^{-2}$) | 4 | $H_2O$ | benzyl alcohol | benzaldehyde | 36 | 96 | >99 | [51b] |
| $Pt-g-C_3N_4$ | 300 W Xe lamp ($\lambda > 400$ nm) | 20 | $H_2O$ | benzyl alcohol | benzaldehyde | 51 | 40 | 90 | [53] |
| $^{NCN}CN_x$-NiP | 1 sun irradiation | 24 | 0.02 M $KP_i$ | 4-methyl-benzyl alcohol | 4-methyl-benzaldehyde | 21.3 | 66.0 | 100 | [55] |
| $CdS/CdO_x$ | solar light (100 mW cm$^{-2}$) | 24 | 10 M KOH | paper | - | 12.37 | - | - | [56a] |
| | | 144 | | α-cellulose | - | 18.42 | 9.21 | - | |
| Co/CdS | 300 W Xe lamp ($\lambda > 420$ nm) | 3 | $CH_3CN$ | benzyl alcohol | benzaldehyde | 202.0 | 18.5 | 94.4 | [59b] |
| Ni/CdS | 8 W blue LED ($\lambda = 450$ nm) | 8 | $H_2O$ | furfural alcohol | furfural | 160.5 | 81.7 | 100 | [63] |
| CdSe-Ni$^{2+}$ | purple LED ($\lambda = 410$ nm) | 6 | $H_2O$ | fenzyl alcohol | benzaldehyde | 87 | 92 | 98 | [65] |
| $Ru/SrTiO_3$:Rh | 300 W Xe lamp ($\lambda > 420$ nm) | 24 | Toluene/ $H_3PO_4$ | (4-methoxyphenyl)-methanol | 4-methoxy benzaldehyde | 247.5 | 92 | 100 | [67] |

## Conclusions

In this Feature Article, we have summarized the recent progress in electrocatalytic and photocatalytic water splitting integrated with organic oxidation for efficient $H_2$ generation and organic transformation. Such a new catalysis strategy is complementary to conventional focus on catalyst design in minimizing the overpotential requirements for both HER and OER in pure water splitting. Instead, it suggests to adopt thermodynamically more favourable organic oxidation reactions to replace OER, which bears several intrinsic advantages, such as eliminating the formation of explosive $H_2/O_2$ mixtures and reactive oxygen species (ROS). Even though such a novel direction in electro- and photocatalysis is still in an early stage, quite a few organic substrates have been explored, including alcohols, ammonia, urea, hydrazine, biomass-derived platform chemicals and even raw biomass materials.

In the electrocatalysis field, earth-abundant materials like first-row transition metals have found promising applications as electrocatalysts for both HER and the accompanying organic oxidation reactions. However, the overpotential requirements for those organic oxidations are still quite high. Given the much lower thermodynamic potentials of those organics relative to that of OER, much smaller oxidation potential should be realized to drive their oxidation. In addition, electrocatalytic selectivity towards the most desirable products should be further improved. In some cases, the poison issue of electrocatalysts by organic substrates could be severe. It is thus a long-term challenge to explore highly efficient, robust, and selective electrocatalysts of low-cost for this coupling electrocatalysis strategy. In order to achieve sufficient conductivity, electrolyte (*i.e.*, KOH) with high concentration is typically required. Therefore, the separation and purification of the obtained organic products from aqueous electrolytes at low cost should also be considered.

In the photocatalysis field, it is exciting to see raw biomass materials could be directly utilized as hole scavengers for photo-induced $H_2$ production. Nevertheless, the scope of explored semiconductors is still limited and most of them do not absorb a large portion of the solar spectrum. Considering the lower oxidizing power requirement of many organic reactions relative to that of water oxidation, it is anticipated that a much larger pool of semiconductors can be considered as candidates for this coupling photocatalysis strategy in the future. Currently, only relatively simple organic oxidations (*i.e.*, alcohol oxidation) have been integrated with $H_2$ evolution in both electrocatalysis and photocatalysis. In order to enlarge the versatility and demonstrate the real potential of this coupling catalysis approach, it is highly desirable to explore more challenging yet useful organic reactions, such as oxidative C-C coupling. One could even envisage coupling both organic reactions to complete the redox cycle of electro- and photocatalysis. In addition, developing efficient and robust membrane to separate the organics should also be taken into account. Overall, along the development of competent catalysts and semiconductors, more exciting results in this burgeoning field of integrating reduction and oxidation reactions in both electrolyzers and photo-reactors can be certainly expected.

## Author contributions

†These authors contributed equally.

ARTICLE

## Conflicts of interest

There are no conflicts to declare.

## Acknowledgements

## Notes and references

1   (a) S. Chu, Y. Cui and N. Liu, *Nat*. *Mater*., 2017, **16**, 16; (b) N. S. Lewis and D. G. Nocera, *Proc*. *Natl*. *Acad*. *Sci*. *U*. *S*. *A*., 2006, **103**, 15729; (c) B. You and Y. Sun, *Acc*. *Chem*. Res., 2018, 51, DOI: 10.1021/acs.accounts.8b00002.

2   (a) B. M. Hunter, H. B. Gray and A. M. Müller, *Chem*. *Rev*., 2016, **116**, 14120; (b) C. G. Morales-Guio and X. Hu, *Acc*. *Chem*. *Res*., 2014, **47**, 2671.

3   (a) Z. W. Seh, J. Kibsgaard, C. F. Dickens, I. Chorkendorff, J. K. Nørskov  and T. F. Jaramillo, *Science*, 2017, **355**, 4998; (b) B. You and Y. Sun, *ChemPlusChem*, 2016, **81**, 1045.

4   (a) S. Chu and A. Majumdar, *Nature*, 2012, **484**, 294; (b) H. B. Gray, *Nat*. *Chem*., 2009, **1**, 7.

5   (a) J. H. Montoya, L. C. Seitz, P. Chakthranont, A. Vojvodic, T. F. Jaramillo and J. K. Nørskov, *Nat*. *Mater*., 2017, **16**, 70; (b) D. G. Nocera, *Acc*. *Chem*. *Res*., 2012, **45**, 767.

6   (a) D. G. Nocera, *Acc*. *Chem*. *Res*., 2017, **50**, 616; (b) T. Asefa, *Acc*. *Chem*. *Res*., 2016, **49**, 1873; (c) V. R. Stamenkovic, D. Strmcnik, P. P. Lopes and N. M. Markovic, *Nat*. *Mater*., 2017, **16**, 57; (d) J. Hwang, R. R. Rao, L. Giordano, Y. Katayama, Y. Yu and Y. Shao-Horn, *Science*, 2017, **358**, 751.

7   M. R Gao, Y. R. Zheng, J. Jiang and S. H. Yu, *Acc*. *Chem*. *Res*., 2017, **50**, 2194.

8   (a)  D. Kang, T. W. Kim, S. R. Kubota, A. C. Cardiel, H. G. Cha and K.-S. Choi, *Chem*. *Rev*., 2015, **115**, 12839; (b) K. Chang, X. Hai and J. Ye, *Adv*. *Energy Mater*., 2016, **6**, 1502555; (c) J. Qi, W. Zhang and R. Cao, *Adv*. *Energy Mater*., 2017, **7**, 1701620; (d) S. Wang and X. Wang, *Small*, 2015, **11**, 3097.

9   M. Carmo, D. L. Fritz, J. Mergel and D. Stolten, *Int*. *J*. *Hydrogen Energy*., 2013, **38**, 4901.

10  J. R. McKone, N. S. Lewis and H. B. Gray, *Chem*. *Mater*., 2014, **26**, 407.

11  (a) B. Rausch, M. D. Symes, G. Chisholm, L. Cronin, *Science*, 2014, **345**, 1326; (b) M. D. Symes and L. Cronin, *Nat*. *Chem*., 2013, **5**, 403; (c) B. Rausch, M. D. Symes, L. Cronin, *J*. *Am*. *Chem*. *Soc*., 2013, **135**, 13656.

12  (a) L. Chen, X. Dong, Y. Wang and Y. Xia, *Nat*. *Commun*., 2016, **7**, 11741; (b) (25)  A. Landman, H. Dotan, G. E. Shter, M. Wullenkord, A. Houaijia, A. Maljusch, G. S. Grader and A. Rothschild, *Nat*. *Mater*., 2017, **16**, 646.

13  W. Li, N. Jiang, B. Hu, X. Liu, F. Song, G. Han, T. J. Jordan, T. B. Hanson, T. L. Liu and Y. Sun, *Chem*, 2018, **4**, 637.

14  Y. X. Chen, A. Lavacchi, H. A. Miller, M. Bevilacqua, J. Filippi, M. Innocenti, A Marchionni, W. Oberhauser, L. Wang and F. Vizza, *Nat*. *Commun*., 2014, **5**, 4036.

15  G. F. Chen, Y. Luo, L. X. Ding and H. Wang, *ACS Catal*., 2018, **8**, 526.

16  T. Wu, X. Zhu, G. Wang, Y. Zhang, H. Zhang and H. Zhao, *Nano Res*., 2018, **11**, 1004.

17  J. Zheng, X. Chen, X. Zhong, S. Li, T. Liu, G. Zhuang, X. Li, S. Deng, D. Mei and J. G. Wang, *Adv*. *Funct*. *Mater*., 2017, **27**, 1704169.

18  (a) L. Dai, Q. Qin, X. Zhao, C. Xu, C. Hu, S. Mo, Y. O. Wang, S. Lin, Z. Tang and N. Zheng, *ACS Cent*. *Sci*., 2016, **2**, 538; (b) X. Zhao, L. Dai, Q. Qin, F. Pei, C. Hu and N. Zheng, *Small*, 2017, **13**, 1602970.

19  W. Xu, R. Lan, D. Du, J. Humphreys, M. Walker, Z. Wu, H. Wang and S. Tao, *Appl. Catal. B-Environ.,* 2017, **218**, 470.

20  J. Gwak, M. Choun and J. Lee, *ChemSusChem*, 2016, **9**, 403.

21  F. Vitse, M. Cooper and G. G. Botte, *J*. P*ower Sources*, 2005, **142**, 18.

22  S. Chen, J. Duan, A. Vasileff and S. Z. Qiao, *Angew*. *Chem*. *Int*. *Ed*., 2016, **55**, 3804.

23  D. D. Zhu, C. Guo, J. Liu, L. Wang, Y. Du and S. Z. Qiao, *Chem*. *Commun*., 2017, **53**, 10906.

24  G. Wang, j. Chen, Y. Li, J. Jia, P. Cai and Z. Wen, *Chem*. *Commun*., 2018, **54**,2603.

25  Y. Tong, P. Chen, M. Zhang, T. Zhou, L. Zhang, W. Chu, C. Wu and X. Xie, *ACS Catal*., 2018, **8**, 1.

26  C. Tang, R. Zhang, W. Lu, Z. Wang, D. Liu, S. Hao, G. Du, A. M. Asiri and X. Sun, *Angew*. *Chem*. *Int*. *Ed*., 2017, **56**, 842.

27  J. Wang, R. Kong, A. M. Asiri and X. Sun, *ChemElectroChem*, 2017, **4**, 481.

28  M. Liu, R. Zhang, L. Zhang, D. Liu, S. Hao, G. Du, A. M. Asiri, R. Kong and X. Sun, *Inorg*. *Chem*. *Front*., 2017, **4**, 420.

29  B. You, N. Jiang, X. Liu and Y. Sun, *Angew*. *Chem*. *Int*. *Ed*., 2016, **55**, 9913.

30  B. You, X. Liu, N. Jiang and Y. Sun, *J*. *Am*. *Chem*. *Soc*., 2016, **138**, 13639.

31  N. Jiang, B. You, R. Boonstra, I. M. T. Rodriguez and Y. Sun, *ACS Energy Lett*., 2016, **1**, 386.

32  N. Jiang, X. Liu, J, Dong, B. You, X. Liu and Y. Sun, *ChemNanoMat*, 2017, **3**, 491.

33  B. You, X. Liu, X. Liu and Y. Sun, *ACS Catal*., 2017, **7**, 4564.

34  (a) S. Hao, L. Yang, D. Liu, R. Kong, G. Du, A. M. Asiri, Y. Yang and X. Sun, *Chem*. *Commun*., 2017, **53**, 5710; (b) M. Wang, J. Ma, H. Liu, N. Luo, Z. Zhao and F. Wang, *ACS Catal*., 2018, **8**, 2129.

35  C. Lyu, J. Zheng, R. Zhang, R. Zou, B. Liu and W. Zhou, *Mater*. *Chem*. *Front*., 2018, **2**, 323.

36  P. Du, J. Zhang, Y. Liu and M. Huang, *Electrochem*. *Commun*., 2017, **83**, 11.

37  K. E. Sanwald, T. F. Berto, W. Eisenreich, A. Jentys, O. Y. Cutiérrez and J. A. Lercher, *ACS Catal*., 2017, **7**, 3236.

38  (a) W. Li, J. Liu and D. Zhao, *Nat*. *Rev*. *Mater*., 2016, **1**, 16023; (b) D. He, K. Cheng, T. Peng, M. Pan and S. Mu, *J*. *Mater*. *Chem*. *A*, 2013, **1**, 2126; (c) B. You, N. Li, H. Zhu, X. Zhu and J. Yang, *ChemSusChem*, 2013, **6**, 474; (d) B. You, Z. Zhang, L. Zhang and J. Yang, *RSC Adv*., 2012, **2**, 5071; (e) B. You, J. Yang, Y. Sun and Q. Su, *Chem*. *Commun*., 2011, **47**, 12364; (f) B. You, L. Wang, L. Yao and J. Yang, *Chem*. *Commun*., 2013, **49**, 5016; (g) B. You, J. Jiang and S. Fan, *ACS Appl*. *Mater*. *Interfaces*, 2014, **6**, 15302; (h) C. Zheng, J. Zhang, Q. Zhang, B. You and G. Chen, *Electrochimica Acta*, 2015, **152**, 216; (i) D. He, Y. Xiong, J. Yang, X. Chen, Z. Deng, M. Pan, Y. Li and S. Mu, *J*. *Mater*. *Chem*. *A*, 2017, **5**, 1930; (j) B. You, Y. Zhang, P. Yin, D. Jiang and Y. Sun, *Nano Energy*, 2018, **48**, 600.

39  (a) X. Zheng, B. Zhang, P. D. Luna, Y. Liang, R. Comin, O. Voznyy, L. Han, F. Pelayo García de Arquer, M. Liu, C. T. Dinh, T. Regier, J. J. Dynes, S. He, H. L. Xin, H. Peng, D. Prendergast, X. Du and E. H. Sargent, *Nat*. *Chem*., 2018, **10**, 149; (b) N. Li, D. K. Bediako, R. G. Hadt, D. Hayes, T, J. Kempa, F. Cube, D. C. Bell, L. X. Chen and D. G. Nocera, *Proc*. *Natl*. *Acad*. *Sci*. *U*. *S*. *A*., 2017, **114**, 1486; (c) V. Vij, S. Sultan, A. M. Harzandi, A. Meena, J. N. Tiwari, W.-G. Lee, T. Yoon and K. S. Kim, *ACS Catal*., 2017, **7**, 7196.

40  (a) J. Sanabria-Chinchilla, K. Asazawa, T. Sakamoto, K. Yamada, H. Tanaka and P. Strasser, *J*. *Am*. *Chem*. *Soc*., 2011, **133**, 5425; (b) D. A. Finkelstein, R. Imbeault, S. Garbarino, L. Roué and D. Guay, *J*. *Phys*. *Chem*. *C*, 2016, **120**, 4717.

41  (a) H. G. Cha and K.-S. Choi, *Nat*. *Chem*., 2015, **7**, 328; (b) P. Gallezot, *Chem*. *Soc*. *Rev*., 2012, **41**, 1538; (c) Y. Kwon, K. J. P. Schouten, J. C. van der Waal, E. Jong and M. T. M. Koper, *ACS Catal*., 2016, **6**, 6704; (d) M. J. Gilkey and B. Xu, *ACS Catal*.,

2016, **6**, 1420; (e) A. M. Robinson, J. E. Hensley and J. W. Medlin, *ACS Catal.*, 2016, **6**, 5026; (f) G. W. Huber, J. N. Chheda, C. J. Barrett and J. A. Dumesic, *Science*, 2005, **308**, 1446.

42 (a) X. Jin, M. Zhao, C. Zeng, W. Yan, Z. Song, P. S. Thapa, B. Subramaniam and R. V. Chaudhari, *ACS Catal.*, 2016, **6**, 4576.; (b) D.-H. Nam, B. J. Taitt and K.-S. Choi, *ACS Catal.*, 2018, **8**, 1197; (c) S. Xu, P. Zhou, Z. Zhang, C. Yang, B. Zhang, K. Deng, S. Bottle and H. Zhu, *J. Am. Chem. Soc.*, 2017, **139**, 14775.

43 (a) N. Jiang, B. You, M. Sheng and Y. Sun, *Angew. Chem. Int. Ed.*, 2015, **54**, 6251; (b) B. You, N. Jiang, M. Sheng, S. Gul, J. Yano and Y. Sun, *Chem. Mater.*, 2015, **27**, 7636; (c) N. Jiang, B. You, M. Sheng and Y. Sun, *ChemCatChem*, 2016, **8**, 106; (d) B. You and Y. Sun, *Adv. Energy Mater.*, 2016, **6**, 1502333; (e) B. You, N. Jiang, M. Sheng, M. W. Bhushan and Y. Sun, *ACS Catal.*, 2016, **6**, 714; (f) X. Liu, B. You and Y. Sun, *ACS Sustainable Chem. Eng.*, 2017, **5**, 4778; (g) X. Liu, J. Dong, B. You and Y. Sun, *RSC Adv.*, 2016, **6**, 73336.

44 (a) J. A. Turner, *Science*, 2004, **305**, 972; (b) A. J. Bard and M. A. Fox, *Acc. Chem. Res.,* 1995, **28**, 141; (c) M. G. Walter, E. L. Warren, J. R. McKone, S. W. Boettcher, Q. Mi, E. A. Santori and N. S. Lewis, *Chem. Rev.,* 2010, **110**, 6446.

45 (a) H. Kim, D. Hwang, Y. Kim and J. Lee, *Chem. Commun.,* 1999, 1077; (b) H. Lu, J. Zhao, L. Li, L. Gong, J. Zheng, L. Zhang, Z. Wang, J. Zhang and Z. Zhu, *Energy Environ. Sci.*, 2011, **4**, 3384.

46 (a) Y. Ma, X. Wang, Y. Jia, X. Chen, H. Han and C. Li, *Chem. Rev.,* 2014, **114**, 9987; (b) Y. Xu, Y. Huang and B. Zhang, *Inorg. Chem. Front.,* 2016, **3**, 591; (c) K. Chang, Z. Mei, T. Wang, Q. Kang, S. Ouyang and J. Ye, *ACS Nano*, 2014, **8**, 7078.

47 A. Fujishima and K. Honda, *Nature*, 1972, **238**, 37.

48 (a) X. Chen, S. Shen, L. Guo and S. S. Mao, *Chem. Rev.,* 2010, **110**, 6503; (b) T. Hisatomi, J. Kubota and K. Domen, *Chem. Soc. Rev.*, 2014, **43**, 7520.

49 (a) G.-J. Ten Brink, I. W. Arends and R. A. Sheldon, *Science*, 2000, **287**, 1636; (b) T. Mallat and A. Baiker, *Chem. Rev.,* 2004, **104**, 3037; (c) S. Yurdakal, G. Palmisano, V. Loddo, V. Augugliaro and L. Palmisano, *J. Am. Chem. Soc.*, 2008, **130**, 1568.

50 (a) M. Zhang, Q. Wang, C. Chen,L. Zang, W. Ma and J. Zhao, *Angew. Chem., Int. Ed.,* 2009, **48**, 6081; (b) U. R. Pillai and E. Sahle-Demessie, *J. Catal.,* 2002, **211**, 434; (c) S. Yurdakal, G. Palmisano, V. Loddo, O. Alagoez, V. Augugliaro and L. Palmisano, *Green Chem.,* 2009, **11**, 510; (d) S. Yurdakal, G. Palmisano, V. Loddo, V. Augugliaro and L. Palmisano, *J. Am. Chem. Soc.,* 2008, **130**, 1568; (e) K. Imamura, H. Tsukahara, K. Hamamichi, N. Seto, K. Hashimoto and H. Kominami, *Appl. Catal. A-Gen.,* 2013, **450**, 28; (f) M. Li, N. Zhang, R. Long, W. Ye, C. Wang and Y. Xiong, *Small,* 2017, **13**, 1604173.

51 (a) W. Zhai, S. Xue, A. Zhu, Y. Luo and T. Tian, *ChemCatChem,* 2011, **3**, 127; (b) S. Higashimoto, Y. Tanaka, R. Ishikawa, S. Hasegawa, M. Azuma, H. Ohue and Y. Sakata, *Catal. Sci. Technol.,* 2013, **3**, 400.

52 (a) Y. Wang, X. Wang and M. Antonietti, *Angew. Chem. Int. Ed.*, 2012, **51**, 68; (b) J. Liu, Y. Liu, N. Liu, Y. Han, X. Zhang, H. Huang, Y. Lifshitz, S.-T. Lee and J. Zhong, Z. Kang, *Science*, 2015, **347**, 970; (c) D. J. Martin, P. J. T. Reardon, S. J. A. Moniz and J. Tang, *J. Am. Chem. Soc.* 2014, **136**, 12568.

53 F. Li, Y. Wang, J. Du, Y. Zhu, C. Xu and L. Sun, *Appl. Catal. B-Environ.,* 2018, **225**, 258.

54 Y. Liu, S. Yang, S.-N. Yin, L. Feng, Y. Zang and H. Xue, *Chem. Eng. J.*, 2018, **334**, 2401.

55 H. Kasap, C. A. Caputo, B. C. M. Martindale, R. Godin, V. W. Lau, B. V. Lotsch, J. R. Durrant and E. Reisner, *J. Am. Chem. Soc.,* 2016, **138**, 9183.

56 (a) K. Akihiko and Y. Miseki, *Chem. Soc. Rev.,* 2009, **38**, 253. (b) Z. Chai, T.-T. Zeng, Q. Li, L.-Q. Lu, W.-J. Xiao and D. Xu, *J. Am. Chem. Soc.*, 2016, **138**, 10128.

57 T. Mitkina, C. Stanglmair, W. Setzer, M. Gruber, H. Kisch and B. König, *Org. Biomol. Chem.,* 2012, **10**, 3556.

58 T. Simon, N. Bouchonville, M. J. Berr, A. Vaneski, A. Adrović, D. Volbers, R. Wyrwich, M. Döblinger, A. S. Susha, A. L. Rogach, F. Jäckel, J. K. Stolarczyk and J. Feldmann, *Nat. Mater.*, 2014, **13**, 1013.

59 (a) T. P. A. Ruberu, N. C. Nelson, I. I. Slowing and J. Vela, *J. Phys. Chem. Lett.,* 2012, **3**, 2798; (b) D. Jiang, X. Chen, Z. Zhang, L. Zhang, Y. Wang, Z. Sun, R. M. Irfan and P. Du, *J. Catal.,* 2018, **357**, 147.

60 D. W. Wakerley, M. F. Kuehnel, K. L. Orchard, K. H. Ly, T. E. Rosser and E. Reisner, *Nat. Energy*, 2017, **2**, 17021.

61 (a) R. F. Service, *Science*, 2009, **324**, 875; (b) X. Huang, S. Li, Y. Huang, S. Wu, X. Zhou, S. Li, C. L. Gan, F. Boey, C. A. Mirkin and H. Zhang, *Nat. Commun.,* 2011, **2**, 292; (c) K. G. Zhou, N. N. Mao, H. X. Wang, Y. Peng and H. L. Zhang, *Angew. Chem. Int. Ed.,* 2011, **50**, 10839.

62 (a) Y. Xu, W. Zhao, R. Xu, Y. Shi and B. Zhang, *Chem. Commun.,* 2013, **49**, 9803; (b) Y. Huang, Y. Xu, J. Zhang, X. Yin, Y. Guo, and B. Zhang, *J. Mater. Chem. A,* 2015, **3**, 19057.

63 G. Han, Y.-H. Jin, R. A. Burgess, N. E. Dickenson, X.-M. Cao and Y. Sun, *J. Am. Chem. Soc.,* 2017, **139**, 15584.

64 P. V. Kamat, K. Tvrdy, D. R. Baker and J. G. Radich, *Chem. Rev.,* 2010, **110**, 6664.

65 L.-M. Zhao, Q.-Y. Meng, X.-B. Fan, C. Ye, X.-B. Li, B. Chen, V. Ramamurthy, C.-H. Tung and L.-Z. Wu, *Angew. Chem. Int. Ed.,* 2017, **56**, 3020.

66 S. Sarina, S. Bai, Y. Huang, C. Chen, J. Jia, E. Jaatinen, G. A. Ayoko, Z. Bao and H. Zhu, *Green Chem.,* 2014, **16**, 331.

67 Z. Liu, J. Caner, A. Kudo, H. Naka, S. Saito, *Chem.-Eur. J.,* 2013, **19**, 9452.

68 Z. Liu, Z. Yin, C. Cox, M. Bosman, X. Qian, N. Li, H. Zhao, Y. Du, J. Li and D. G. Nocera, *Sci. Adv.,* 2016, **2**, e1501425.
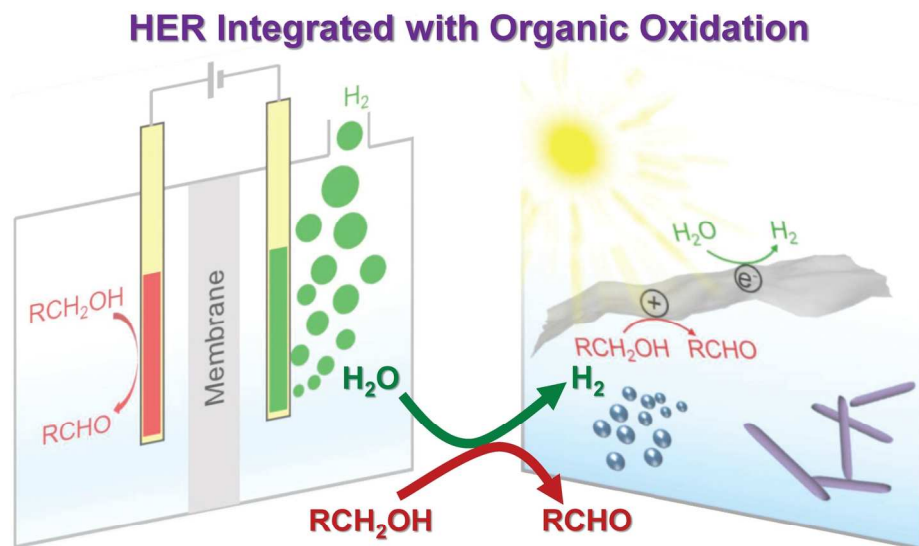
Dr. Bo You received his B.S. degree in Chemistry from Heilongjiang University in 2008 and a Ph.D. degree under the supervision of Prof. Zhaoxiang Deng at University of Science and Technology of China in 2014. Subsequently, he conducted a postdoctoral research in Prof. Yujie Sun's group at Utah State University. His research interest is interface catalysis for advanced renewable energy (ICARE).



Guanqun Han received her B.S. degree in Polymer Materials and Engineering from Qingdao University of Science and Technology in 2012 and her M.S. degree in Chemistry from China University of Petroleum (East China) in 2016. Since then, she is pursuing her Ph.D degree at Utah State University under the supervision of Prof. Yujie Sun. Her research interests include inexpensive heterogeneous catalysts for $H_2$ evolution and organic upgrading.
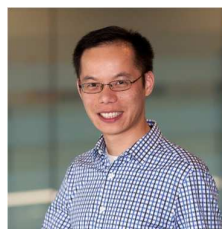


Dr. Yujie Sun received a B.S. degree in Chemistry from Fudan University in 2005. He then pursued graduate studies in inorganic photochemistry with Prof. Claudia Turro at The Ohio State University and received a Ph.D. degree in 2010. Subsequently, he joined the group of Prof. Chris Chang at the University of California, Berkeley and Lawrence Berkeley National Laboratory for postdoctoral studies. In 2013, Yujie started his independent career as an assistant professor at Utah State University. His group is interested in developing and understanding inexpensive materials and complexes for energy catalysis and biomedical applications.

161x114mm (300 x 300 DPI)